HOSTED BY

ELSEVIER

Available online at www.sciencedirect.com

ScienceDirect

Resource-Efficient Technologies 1 (2015) 34–48

www.elsevier.com/locate/reffit

Review article

# Induced polarization effect in reservoir rocks and its modeling based on generalized effective-medium theory

Vladimir Burtman [a,b,*], Michael S. Zhdanov [a,b,c]

[a] Geology and Geophysics Department, University of Utah, 115 S 1460 E, ROOM 383, Salt Lake City, UT 84112-0102, USA
[b] TechnoImaging LLC, 4001 South 700 East, Salt Lake City, UT 84107, USA
[c] Moscow Institute of Physics and Technology, Institutskiy per., 9, Moscow, Russia

Received 7 April 2015; received in revised form 19 June 2015; accepted 20 June 2015

Available online 16 July 2015

**Abstract**

One of the major tasks of the petroleum resource-efficient technologies (pREFFIT) is the development and improvement of the methods of exploration for energy resources. This review paper summarizes the results of the research on induced polarization (IP) effect in reservoir rocks conducted by the University of Utah Consortium for Electromagnetic Modeling and Inversion (CEMI) and TechnoImaging. The electrical IP effect in hydrocarbon (HC) bearing reservoir rocks having nonmetallic minerals is usually associated with membrane polarization, which is caused by a variation in the mobility of the ions throughout the rock structure. This mobility is related to the size and shape of the pores filled with electrolyte and the double electrical layers. We have studied the IP response of multiphase porous systems by conducting complex resistivity (CR) frequency-domain IP measurements for two different groups of samples: sands and sandstones containing salt water in pores and those whose unsaturated pores were filled with synthetic oil. We have also studied selected carbonate reservoir formations, typical of some major HC deposits. The generalized effective-medium theory of induced polarization (GEMTIP) was used to analyze the IP parameters of the measured responses. This paper presents a conceptual model of polarizing clusters to explain the observed IP phenomena. The results of this study show that the HC bearing sands and sandstone samples and carbonate rocks are characterized by a significant IP response. These experimental observations, compared with the theoretical modeling based on the GEMTIP approach, confirm earlier geophysical experiments with the application of the IP method for HC exploration.



*Keywords:* EM exploration; Complex resistivity; Induced polarization; Unconventional energy resources; Effective-medium theory; CEMI; REFFIT

## 1. Introduction

The induced polarization (IP) effect is widely used in mining applications in search of mineral resources. Until recently, the IP method did not find wide application in the petroleum industry due to the complexity and ambiguity of interpretation results. However, recent improvements in IP data acquisition and interpretation have stimulated a renewed interest in its use in hydrocarbon (HC) exploration.

The measurement of the electrical IP effect has proven to be one of a few geophysical methods providing in situ information about rock mineralogy, especially in the search for disseminated minerals with electronic conductivity. At the same time, the method has been applied to study the earth materials that do not contain conductive minerals, like sedimentary rocks. The method has been used, though rarely, in the fields of hydrology [1,2], hydrocarbon (HC) exploration [3,4] and in environmental studies such as mapping of polluted land areas [5]. It is worth noting that previous IP studies of nonmetallic earth materials were focused on clay mineral soils, sandy and shaly sediments containing clay minerals [6]. Laboratory studies of the electrical characteristics of such rocks show diagnostic signatures of what they consist of and, thus, can lead to a proper classification of rocks in terms of the presence of clay and other materials. At the same time, the study of reservoir rocks was limited and did not include a quantitative analysis of the relationships between the petrophysical parameters of the rock samples and the IP responses.

The IP effect is a geophysical phenomenon which is manifested by the slow decay of voltage in the ground after the cessation of an excitation current pulse (time domain method) or

* Corresponding author. 115 S 1460 E, ROOM 383, Geology and Geophysics Department, University of Utah, Salt Lake City, UT 84112-0102, USA. Tel.: +1 8012442693; fax: +1 8012646708.
*E-mail address:* vlad.burtman@gmail.com (V. Burtman).

http://dx.doi.org/10.1016/j.reffit.2015.06.008

low frequency variation of the resistivity of the earth (frequency domain method) [7]. In simple terms, the IP effect reflects the degree to which the subsurface is able to store electric charge, analogous to a leaky capacitor. It occurs when an electric current passes through a rock or soil. If the current is interrupted, a difference in potential, which decays with time, is observed. The rate of decay of this potential (induced polarization potential) depends on the lithology of the rock, its pore geometry, and the degree of water and HC saturation. It was noted in the pioneering paper by Conrad Schlumberger (1920) [8] that this phenomenon was taking place in the bulk volume of the rock and not on the electrodes used to measure it. In an attempt to describe the observed phenomenon, he attributed the transient voltage to an electrical polarization of the ground and thus used the same phenomenon in exploiting and locating unexposed ores. The dependency of the polarizability of rocks/soils upon their lithological composition and hydrogeological properties favors the application of the IP method for hydrogeological (groundwater) and engineering geologic investigations. The polarization phenomenon was previously studied in detail by Wait (1959) [9] and its modern development stems largely from the work done by Bleil (1953) [10].

Vacquier et al. (1957) [1] and Marshall and Madden (1959) [2] described, respectively, the time domain IP measurements on artificial clay and sand mixtures and a theoretical model for membrane (clay) polarization. Ogilvy and Kuzmina (1972) [11] described additional time domain measurements on artificial mixtures, while Roy and Elliot (1980) [12] used horizontal layers of varying clay–sand composition to model negative apparent chargeabilities due to geometric effects. Vanhala and Soininen (1995) [13] carried out laboratory measurements using spectral IP on soil samples in order to assess the effect of mineralogy, grain size distribution, moisture content, and electrolyte composition on the resistivity of soil material. Rocks, which contain clay minerals, often display electrical properties which cannot be predicted by the bulk electrical properties of the constituents [14]. Interactions between clay minerals and ground water can produce polarization phenomena and decrease the resistivity.

The electrical resistivity of the reservoir rocks depends directly on the electrical resistivity and fluid saturation of the pores, as well as the clay (sands or zeolite) content. When clay is present, the resistivity becomes frequency dependent because of a fundamental charge storage mechanism that introduces double layers of electrical charge and a capacitive-like element in the equivalent circuit representation of the rock. Vacquier et al. (1957) [1] studied the membrane polarization effect in groundwater prospecting. He found that the ratio of two chargeability values measured at different times after cut-off of the current pulse, i.e., a quantity roughly dependent on the relaxation time, could be related to the grain size of the sediment. Marshall and Madden (1959) [2] presented a membrane-polarization model which, although an ultimate simplification for sediment texture, gave qualitatively correct predictions of how grain size affects the phase spectrum of the sediment.

As we discussed above, the IP effect is caused by the concentration gradients that develop at solid and liquid phase boundaries in response to the current flow. This effect is especially strong in the presence of clay materials. Keller and Frischknecht (1966) [15] made a qualitative development of this concept based on anion blockage to demonstrate that theoretically there is a peak polarization response for different clays and their concentrations. The variation in the intensity of polarization implies that clay content also changes from place to place in the rock.

The dependency of resistivity on clay type and content has been used as a parameter for a prediction of porosity and hydrocarbon saturation from well logs. Waxman and Smits (1968) [16] and Waxman and Thomas (1974) [17] have assumed that the resistivity of rocks is frequency dependent, which is true at low frequencies. They developed a semi-empirical model for describing the dependence of resistivity on clay content, expressed as CEC per unit volume. Vacquier et al. (1957) [1] found that the chargeability of sand–clay mixtures was proportional to the constituent clay and its ionic exchange characteristics. The importance of rock texture for the IP effect is manifested by a weak IP in compact clays (low CEC), and a strong IP in sediments with disseminated clay particles (high CEC) on the surface of larger grains. Increased electrolyte salinity (ion concentration) and electrical conductivity decrease the IP effect [6].

Parkhomenko (1971) [18] found that for fixed clay content, the chargeability of a rock is greater for clays having higher ion exchange capacities. However, this does not apply in the case of massive or pure clay. She observed that the largest IP effects were obtained for clay contents in the range of 3–10%. Higher or lower clay content corresponded to a lower IP effect. Parkhomenko (1971) [18] also noted that the IP effect increased with increasing water content until an optimum saturation is reached, beyond which IP decreased. The salinity and composition of the electrolyte have a profound influence upon the mode of occurrence of this maximum. With increasing concentration, the maximum IP response is depressed and shifts slightly toward the lower water contents. In a study with shaly sands, Ogilvy and Kuzmina (1972) [11] demonstrated the occurrence of a maximum IP response for optimum water content.

Keller and Frischknecht, 1966 [15], and Ogilvy and Kuzmina, 1972 [11], studied the effect of grain size parameters on the IP response. They have reported that the IP effect is low in the extreme cases of clean gravels or pure shales but it attains a maximum value at some intermediate grain size. Dakhnov (1962) [19] found that, with the fully saturated reservoir rock, the IP response was approximately proportional to the specific surface area of the constituent grains. It must be noted that this specific surface area increases with a decrease in grain size.

De Lima and Sharma (1992) [20] demonstrated that a model of a membrane polarization phenomenon could be reduced to a Cole–Cole model. Boadu and Seabrook (2000) [21] used a double Cole–Cole model to explain a laboratory measurement on the soil samples which showed a frequency dependent electrical response (FDER). They have demonstrated that the FDER resistivity and phase spectra of the soil contain valuable information about its porosity, hydraulic conductivity, texture, and fluid properties.

The first systematic experimental attempt to demonstrate that the IP effect is actually an intrinsic property of petroleum was accomplished in mid 1980s [22]. The transport properties

of soils and rocks such as fluid-flow permeability and electrical conductivity are also important in near-surface environmental and engineering applications [23,24]. Wet, porous soils are generally very heterogeneous multiphase systems with a complicated internal structure whose electrical and hydraulic properties depend on the pore space geometry and are also related to the microstructure of the pore space. The polarization and the complex nature of electrical rock conductivity are attributed to zones of unequal ionic transport properties along the pore channels caused by charged interfaces and constrictions. The interactions at and near the contact area of the solid and liquid phases are the main causes of the formation of electrical double layers. The various electrical phase boundary phenomena are of special interest, because they result in a dispersion of the electrical conductivity in the frequency range from 1 mHz to 10 kHz [22]. Eventually Dobecki and Roming (1985) [25], and Tune and Daggar (1990) [26] were the first who reported an application of the IP method in nonmetalliferous environments.

Due to the complexity and ambiguity of interpretation results, the IP method did not find wide application in the petroleum industry. Recent improvements in data acquisition and interpretation, and the encouraging practical results obtained recently using the IP method have stimulated a renewed interest in its use in HC exploration [27,28].

In 2006 the Consortium for Electromagnetic Modeling and Inversion (CEMI) at the University of Utah and TechnoImaging initiated a systematic study of IP phenomena in reservoir rocks. The theoretical foundations of the IP effect in complex multiphase heterogeneous rocks were developed by Zhdanov (2006; 2008; 2009) [28–31]. We have also studied the IP effect in multiphase porous rocks in view of possible application in a HC exploration. The results of this study demonstrated that a resistivity of reservoir rocks saturated with the mixture of water and oil is complex and frequency dependent and that the oil-saturated sands and sandstone samples can be characterized by a significant IP response [32–34]. Similar results were also reported in the papers by Revil et al. (2012, 2013) [35,36].

This review paper describes the major milestones of CEMI studies of the IP effect in reservoir rocks from initial feasibility studies to examples of practical applications of developed models and experimental routines. We summarize the basic principles of the generalized effective-medium theory of the IP effect (GEMTIP) developed by Zhdanov (2006, 2008) [29–31]. We demonstrate that, first, the GEMTIP model could be applied to reservoir rocks. Second, we present the results of the lab measurements of the IP effect on the reservoir rocks saturated with the mixture of oil and water, and we show that the GEMTIP model provides an adequate description of the complex resistivity in the rock samples. These experiments were conducted with different HC samples, solid and liquids, and with reservoir rocks of different types, including artificial rocks fabricated from materials that enabled us to have a full control on sample composition. Third, we have found that the GEMTIP model could be used to determine the petrophysical properties of reservoir rocks from the recorded IP data.

## 2. Development of an effective-medium model for reservoir rocks

### 2.1. Basic formulas of the effective-medium theory of induce polarization

The induced polarization (IP) effect is one of the most intriguing phenomena being studied in electromagnetic geophysics. It was emphasized in the original papers by Zhdanov (2008) [30,31] that a comprehensive model of the IP effect should include the electrochemical and electromagnetic aspects of the problem. Acknowledging the complexity of the IP phenomenon, we should consider also the importance of constructing a rigorous physical–mathematical model of heterogeneous multiphase conductive media based on the effective-medium approach, which takes into account both the electromagnetic induction and induced polarization effects.

In the paper by Zhdanov (2008) [30], the author used the classical effective-medium theory approach based on the substitution of a locally homogeneous medium for the heterogeneous multiphase medium typical for rock formations. As a result, the substance, e.g. the porous medium, was represented by a solid medium, which was characterized electromagnetically in terms of a minimum number of parameters of the effective-medium model. The generalized effective-medium model of the IP effect (the GEMTIP model) was based on an assumption that, in addition to electrical heterogeneity, the medium was characterized by polarizability effects, which were manifested by the charge polarization and formation of the electrical double layers in the polarized medium. We present below a short overview of the GEMTIP model.

In the framework of the GEMTIP model, we represent a complex heterogeneous rock formation as a composite model formed by a homogeneous host medium of a volume $V$ with a complex conductivity tensor $\hat{\sigma}_0(r)$ (where $\mathbf{r}$ is an observation point) filled with grains of arbitrary shape and conductivity. In the present problem, the rock is composed of a set of $N$ different types of grains, the $l$th grain type having a complex tensor conductivity $\hat{\sigma}_l$. The grains of the $l$th type have a volume fraction $f_l$ in the medium and a particular shape and orientation. In order to find the effective conductivity tensor $\hat{\sigma}_e$, we represent the given inhomogeneous composite model as a superposition of a homogeneous infinite background medium with the conductivity tensor $\hat{\sigma}_b$ and the anomalous conductivity $\Delta\hat{\sigma}(r)$:

$$\hat{\sigma}(r) = \hat{\sigma}(r)_b + \Delta\hat{\sigma}(r) \tag{1}$$

Following Zhdanov [29–31], we can write the following expression for the effective conductivity of the polarized inhomogeneous medium:

$$\hat{\sigma}_e = \hat{\sigma}_0 + \sum_{l=1}^{N}\left[\hat{I} + \hat{p}_l\right]^{-1}\left[\hat{I} - \Delta\hat{\sigma}_l^p(r)\hat{\Gamma}_l\right]^{-1}\cdot\left[\hat{I} + \hat{p}_l\right]\cdot\Delta\hat{\sigma}_l f_l,$$

where $\hat{\sigma}_e$ is an effective-medium conductivity tensor; $\Delta\hat{\sigma}_l$ is an anomalous conductivity tensor; $\Delta\hat{\sigma}_l^p = \left[\hat{I} + \hat{p}_l\right]\cdot\Delta\hat{\sigma}_l$ is the polarized anomalous conductivity; $\hat{p}_l$ is a surface polarizability

tensor; $\hat{\Gamma}_l$ is a volume depolarization tensor; and index $l$ corresponds to the grain of the $l$th type.

Table 1 presents a list of variables used in this paper.

In particular, if we select the background conductivity to be equal to the host medium conductivity:

$\hat{\sigma}_e = \hat{\sigma}_0$, then:

$$\hat{\sigma}_e = \hat{\sigma}_0 + \sum_{l=1}^{N}\left[\hat{I} + \hat{p}_l\right]^{-1}\left[\hat{I} - \Delta\hat{\sigma}_l^p(r)\hat{\Gamma}_l\right]^{-1}\cdot\left[\hat{I} + \hat{p}_l\right]\cdot\Delta\hat{\sigma}_l f_l, \quad (2)$$

because $\Delta\hat{\sigma}_0 = 0$.

The last formula provides a general solution of the effective conductivity problem for an arbitrary multiphase composite polarized medium. This formula allows us to find the effective conductivity for inclusions with arbitrary shape and electrical properties. That is why the new composite geoelectrical model of the IP effect may be used to construct the effective conductivity for realistic rock formations typical for mineralization zones and/or petroleum reservoirs.

### 2.2. Effective resistivity of the isotropic medium filled with isotropic grains of arbitrary shape: anisotropy effect

We consider first a composite model with isotropic grains of arbitrary shape. In this case all conductivities become scalar functions:

$$\hat{\sigma}_0 = \hat{\mathbf{I}}\sigma_0,\ \Delta\hat{\sigma}_l = \hat{\mathbf{I}}\Delta\sigma_l,\ \Delta\hat{\sigma}_l{}^p = \left(\hat{\mathbf{I}} + \hat{p}_l\right)\Delta\sigma_l.$$

Table 1
List of variables.

| | |
|---|---|
| $\hat{\sigma}$ | Total conductivity tensor |
| $f_l$ | Volume fraction of a grain of the $l$th type |
| $\hat{\sigma}_0$ | Conductivity tensor of host medium |
| $\hat{\sigma}_l$ | Conductivity tensor of a grain of the $l$th type |
| $\hat{\sigma}_e$ | Effective conductivity of the polarized inhomogeneous medium |
| $\Delta\hat{\sigma}$ | Anomalous conductivity tensor |
| $\aleph$ | Complex anisotropy coefficient |
| $k$ | Surface polarizability factor |
| $\theta^i$ | Anisotropy disorder parameter |
| $\hat{\mathbf{G}}_b$ | Green's tensor for the homogeneous background full space |
| $\hat{\Gamma} = \iiint_V \hat{\mathbf{G}}_b d\upsilon$ | Volume depolarization tensor |
| $\hat{\Lambda} = \iint_S \hat{\mathbf{G}}_b \cdot \mathbf{n}\,\mathbf{n} ds$ | Surface depolarization tensor |
| $\hat{\xi} = \kappa\sigma_b\hat{\boldsymbol{\sigma}}\cdot(\Delta\hat{\sigma})^{-1}$ | Relative conductivity tensor |
| $\hat{\mathrm{p}} = \hat{\Gamma}^{-1}\cdot\hat{\Lambda}\cdot\hat{\xi}$ | Surface polarizability tensor |
| $\hat{\mathrm{q}} = \left[\hat{\mathbf{I}} + \hat{\mathrm{p}}\right]\cdot\hat{\mathrm{m}}$ | Volume polarizability tensor |
| $\Delta\hat{\sigma}^p = \left[\hat{\mathbf{I}} + \hat{\mathrm{p}}\right]\cdot\Delta\hat{\sigma}$ | "Polarized" anomalous conductivity |
| $\rho_0$ | DC resistivity |
| $\omega$ | Angular frequency |
| $\tau$ and $C$ | Time and relaxation parameters |
| $\alpha$ | Surface polarizability coefficient |
| $a_x, a_y, a_z$ | Equatorial and polar radii of the ellipsoidal grains |
| $e$ | Eccentricity of the rotational ellipsoid |
| $\varepsilon = a_z/a_x = a_z/a_y$ | Ellipticity of the rotational ellipsoid |

Therefore, we can write:

$$\hat{\sigma}_e = \hat{\mathbf{I}}\hat{\sigma}_0 + \sum_{l=1}^{N}\left[\hat{\mathbf{I}} + \hat{p}_l\right]^{-1}\left[\hat{\mathbf{I}} - \left(\hat{\mathbf{I}} + \hat{p}_l\right)\Delta\hat{\sigma}_l\hat{\Gamma}_l\right]^{-1}\cdot\left[\hat{\mathbf{I}} + \hat{\mathbf{p}}_l\right]\cdot\Delta\sigma_l f_l, \quad (3)$$

where, according to the definition of the surface polarizability tensor (see Table 1):

$$\hat{\mathrm{p}}_l = \hat{\Gamma}_l^{-1}\cdot\hat{\Lambda}_l\cdot\hat{\xi}_l, \quad (4)$$

and $\xi_l$ is equal to:

$$\xi_l = \kappa_l\sigma_0\boldsymbol{\sigma}_l\cdot(\Delta\sigma_l)^{-1}. \quad (5)$$

It can be demonstrated that, if the grains have nonisometric shape (e.g., ellipsoidal shape) but random orientation (see Fig. 1), averaging of the tensor terms in expression (3) will result in scalarization. Therefore, the effective medium conductivity will become a scalar function. However, if all the grains are oriented in one specific, the effective conductivity of this medium will become anisotropic. Thus, the effective conductivity may be a tensor in spite of the fact that the background medium and all the grains are electrically isotropic.

### 2.3. Multiphase heterogeneous medium filled with ellipsoidal inclusions

#### 2.3.1. Effective conductivity of the multiphase composite polarized medium with ellipsoidal inclusions

We consider again an isotropic multiphase composite model. We assume now, however, that all grains have an ellipsoidal shape, and their axes are parallel to one another. It is clear that in this situation, similar to the case of the conventional effective-medium theory without IP effects [37], the effective medium becomes anisotropic. The depolarization tensors of the ellipsoidal grain can

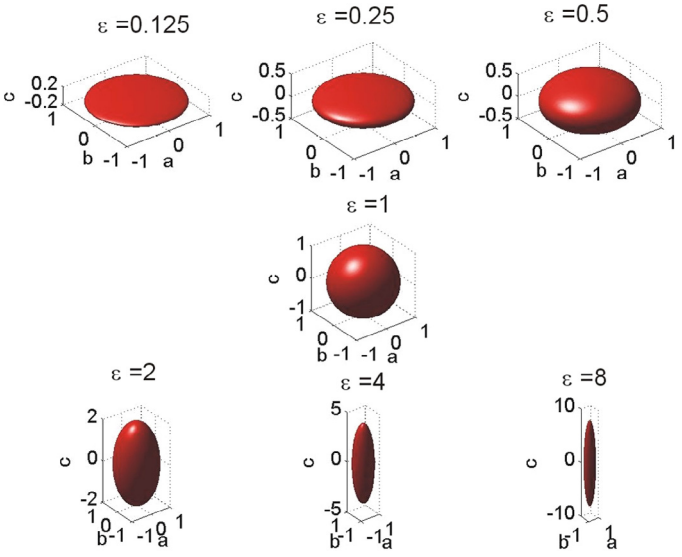


Fig. 1. Typical rotational ellipsoids for different values of the ellipticity ε = c/a, ranging from 0.125 to 8.

be determined according to theory developed in Zhdanov (2008) [30].

Recall formula (3) for the effective conductivity of the isotropic medium filled with isotropic grains of arbitrary shape. Substituting expressions (4) and (5) for the surface polarizability tensor in that formula, we can write:

$$\hat{\sigma}_e = \hat{\mathbf{I}}\sigma_0 + \sum_{l=1}^{N}\left[\hat{\mathbf{I}} + \hat{\Gamma}_l^{-1}\cdot\hat{\Lambda}_l\cdot\xi_l\right]^{-1}$$
$$\left[\hat{\mathbf{I}} - \left(\hat{\mathbf{I}} + \hat{\Gamma}_l^{-1}\cdot\hat{\Lambda}_l\cdot\xi_l\right)\Delta\sigma_l\hat{\Gamma}_l\right]^{-1}\left[\hat{\mathbf{I}} + \hat{\Gamma}_l^{-1}\cdot\hat{\Lambda}_l\right]\Delta\sigma_l f_l =$$
$$\hat{\mathbf{I}}\sigma_0 + \sum_{l=1}^{N}\left[\hat{\mathbf{I}} - \left(\mathbf{I} + \hat{\Gamma}_l^{-1}\cdot\hat{\Lambda}_l\cdot\xi_l\right)\Delta\sigma_l\hat{\Gamma}_l\right]^{-1}\Delta\sigma_l f_l, \quad (6)$$

where we take into account that both the volume, $\hat{\Gamma}_l$, and surface, $\hat{\Lambda}_l$, depolarization tensors become diagonal in the Cartesian system of coordinates (x, y, z) aligned with the axes of ellipsoidal grains:

$$\hat{\Gamma}_l = -\frac{1}{\sigma_0}\hat{\gamma}_l = -\frac{1}{\sigma_0}\begin{bmatrix}\gamma_{lx} & 0 & 0\\ 0 & \gamma_{ly} & 0\\ 0 & 0 & \gamma_{lz}\end{bmatrix} \quad (7)$$

and

$$\hat{\Lambda}_l = -\frac{1}{\sigma_0}\begin{bmatrix}\lambda_{lx} & 0 & 0\\ 0 & \lambda_{ly} & 0\\ 0 & 0 & \lambda_{lz}\end{bmatrix},$$

where the scalar coefficients $\gamma_{lx}$, $\gamma_{ly}$, $\gamma_{lz}$, $\lambda_{lx}$, $\lambda_{ly}$ and $\lambda_{lz}$ are defined by geometrical parameters of the grains.

In the case of spheroidal-shape grains:

$$\hat{\Gamma}_l = -\frac{1}{\sigma_0}\hat{\gamma}_l = -\frac{1}{2\sigma_0}\begin{bmatrix}(1-\gamma_l) & 0 & 0\\ 0 & (1-\gamma_l) & 0\\ 0 & 0 & (1-\gamma_l)\end{bmatrix}, \quad (8)$$

where we assume that the axis $z$ is aligned with the axis of revolution of the ellipsoid, and the equatorial ($a_{lx}$ and $a_{ly}$) radii of the ellipsoidal grains are equal ($a_{lx} = a_{ly} = a_{lz}$ and $a_{lz} = b_l$).

The value of $\gamma_l$ is determined by the eccentricity, $e_l$ of a spheroid. For example, in the case of the prolate spheroid ($b_l > a_l$) with $e_l = \sqrt{1 - a_l/b_l}$, we have:

$$\gamma_l = \frac{1-e_l^2}{e_l^3}\left(\tanh^{-1} e_l - e_l\right). \quad (9)$$

Note that, if $e_l \to 1$, the spheroid transforms into a long thin rod.

For the oblate spheroid $b_l < a_l$ with eccentricity $e_l = \sqrt{a_l/b_l - 1}$, we have:

$$\gamma_l = \frac{1-e_l^2}{e_l^3}\left(e_l - \tanh^{-1} e_l\right). \quad (10)$$

We show in Fig. 1, as an example, typical rotational ellipsoids for different values of the ellipticity $\varepsilon = c/a$, ranging from 0.125 to 8.

The surface depolarization tensor for spheroidal-shape grains is equal to:

$$\hat{\Lambda}_l = -\frac{1}{\sigma_0}\begin{bmatrix}\lambda_l & 0 & 0\\ 0 & \lambda_l & 0\\ 0 & 0 & \lambda_{lz}\end{bmatrix},$$

where $\lambda_l = \lambda_{lx} = \lambda_{ly}$, and $\lambda_{lz}$ can be calculated using the integrals as in Zhdanov (2008) [30].

Therefore, we can rewrite formula (6) using scalar notations:

$$\sigma_{e\alpha} = \sigma_0 + \sum_{l=1}^{N}\left[1 + \left(1 + \gamma_{l\alpha}^{-1}\cdot\lambda_{l\alpha}\cdot\xi_l\right)\frac{\sigma_l}{\sigma_0}\gamma_{l\alpha}\right]^{-1}(\sigma_l - \sigma_0)f_l$$
$$= \sigma_0 + \sum_{l=1}^{N}\left[1 + \left(1 + k_l\sigma_0\sigma_l(\sigma_l - \sigma_0)^{-1}\gamma_{l\alpha}^{-1}\lambda_{l\alpha}\right)\frac{\sigma_l - \sigma_0}{\sigma_0}\gamma_{l\alpha}\right]^{-1}$$
$$(\sigma_l - \sigma_0)f_l, \alpha = x, y, z \quad (11)$$

Thus, we can see that the effective conductivity of the multiphase composite polarized medium with ellipsoidal inclusions aligned along axis z can be represented as a diagonal conductivity tensor:

$$\hat{\sigma}_e = \begin{bmatrix}\sigma_{lx} & 0 & 0\\ 0 & \sigma_{ly} & 0\\ 0 & 0 & \sigma_{lz}\end{bmatrix}. \quad (12)$$

Multiplying the numerator and denominator of every term under a summation sign in (11) by $\rho_l\rho_0$ (where $\rho_0 = 1/\sigma_0$, $\rho_l = 1/\sigma_l$), we obtain an equivalent expression for the effective resistivity of the composite polarized medium:

$$\rho_{e\alpha} = \rho_0\left\{1 + \sum_{l=1}^{N}\left[f_l\frac{\rho_0 - \rho_l}{\rho_l - \gamma_{l\alpha}(\rho_0 - \rho_l) + k_l\lambda_{l\alpha}}\right]\right\}^{-1}, \alpha = x, y, z \quad (13)$$

The last formula results in the following effective resistivity tensor:

$$\hat{\rho}_e = \begin{bmatrix}\rho_{lx} & 0 & 0\\ 0 & \rho_{ly} & 0\\ 0 & 0 & \rho_{lz}\end{bmatrix}. \quad (14)$$

According to the experimental data, the surface polarizability factor is a complex function of frequency [38]. Following Wait (1982) [39] and Zhdanov (2008) [30,31] we use the model:

$$k_l = \alpha_l(i\omega)^{-C_l}, \quad (15)$$

which fits the experimental data, where $\alpha_l$ is some empirical surface polarizability coefficient, measured in the units $[\alpha_l] = (\text{Ohm}\times\text{m}^2)/\text{s}^{Cl}$, and $C_l$ is the relaxation parameter of the $l$th grain.

In the case of spherical grains, the surface polarizability coefficients can be selected in the form [30,31]:

$$\alpha_l = \frac{a_l}{2}(2\rho_l + \rho_0)(\tau_l)^{-C_l}, \quad (16)$$

where $\tau_l$(s) is the time parameter of the $l$th grain. By analogy, in the case of ellipsoidal grains, we define the empirical surface polarization coefficient $\alpha_l$ as:

$$\alpha_l = \frac{\bar{a}_l}{2}(2\rho_l + \rho_0)(\tau_l)^{-C_l}, \tag{17}$$

where $\bar{a}_l$ is an average value of the equatorial ($a_{lx}$ and $a_{ly}$) and polar ($a_{lz}$) radii of the ellipsoidal grains, i.e.:

$$\bar{a}_l = \left(\frac{a_{lx} + a_{ly} + a_{lz}}{3}\right). \tag{18}$$

Substituting formula (15) into expression (13), after some algebra, we have:

$$\rho_{e\alpha} = \rho_0 \cdot \left\{1 + \sum_{l=1}^{N}\left[f_l \frac{\rho_0 - \rho_l}{\rho_l + \gamma_{l\alpha}(\rho_0 - \rho_l) + \bar{a}_l(\rho_l + \rho_0/2)(i\omega\tau_l)^{-C_l}\lambda_{l\alpha}}\right]\right\}^{-1}, \quad \alpha = x, y, z \tag{19}$$

The last formula provides a general solution of the effective resistivity problem for a multiphase composite anisotropic medium filled with ellipsoidal inclusions.

### 2.3.2. Two-phase composite polarized medium with ellipsoidal inclusions

In the case of a two-phase composite model, we have a homogeneous host medium of a volume $V$ with a complex resistivity $\rho_0$ and ellipsoidal inclusions with resistivity $\rho_l$. Formula (13) is simplified:

$$\rho_{e\alpha} = \rho_0\left\{1 + f_l \frac{\rho_0 - \rho_l}{\rho_l + \gamma_{l\alpha}(\rho_0 - \rho_l) + k_l\lambda_{l\alpha}}\right\}^{-1}, \alpha = x, y, z \tag{20}$$

After some algebra we arrive at the formula:

$$\rho_{e\alpha} = \rho_0\left\{1 + f_l \frac{f_l(\rho_0 - \rho_l)}{\rho_l + \gamma_{l\alpha}(\rho_0 - \rho_l) + k_l\lambda_{l\alpha} + f_l(\rho_0 - \rho_l)}\right\}, \quad \alpha = x, y, z \tag{21}$$

and expression (12) takes the form:

$$\rho_{e\alpha} = \rho_0\left\{1 - \frac{f_l(\rho_0 - \rho_l)}{\rho_l + \gamma_{l\alpha}(\rho_0 - \rho_l) + \bar{a}_l(\rho_l + \rho_0/2)(i\omega\tau_l)^{-C_l}\lambda_{l\alpha} + f_l(\rho_0 - \rho_l)}\right\}, \quad \alpha = x, y, z \tag{22}$$

Formula (22) provides an analytical expression for the components of the effective conductivity tensor of two-phase composite polarized medium with the ellipsoidal inclusions oriented along the axis of the Cartesian coordinates $x$, $y$, $z$.

We present below some typical GEMTIP resistivity relaxation models for the two-phase composite polarized media. The models are formed by a homogeneous host rock with a resistivity $\rho_0$ filled with ellipsoidal grains. The resistivities of the host rock and of the grains are $\rho_0 = 2$ Ω-m and $\rho_l = 0.2$ Ω-m, respectively. The volume fraction of grain $f_l$ is equal to 0.05; the time parameter, $\tau_l$, and the relaxation parameter, $C_l$, are equal to: $\tau_l = 0.4$ s; $C_l = 0.8$.

We select the horizontal (equatorial) radius of the rotational ellipsoid, $a$, equal to 1.25 cm, while the vertical (polar) axis, $b$, is variable, depending on the ellipticity ε. The effective resistivity was calculated for the following values of the ellipticity ε = b/a = 5; 0.25; 0.5; 1; 2; 4; 8, as shown in Fig. 2. The plots in the top parts of the panels (a), (b), and (c) represent the real parts of the effective resistivity, while the bottom parts of the same panels show the imaginary parts. For comparison, the bold curves in these plots show the effective resistivity of the isotropic two-phase medium filled with spherical grains. One can clearly see that the presence of the ellipsoidal grains results in an anisotropy effect in the effective resistivity.

### 2.4. A GEMTIP model for membrane polarization

We applied the principles of the generalized effective-medium theory [30] to analyze and interpret the observed data. Fig. 3 summarizes the GEMTIP models used for data analysis.

We considered a polarizable effective medium, which is formed by sand clusters [40], covered by a layer of conductive saltwater and oil matrix. In this effective medium, the saltwater-filling space is considered as a "conductive grain," which sustains the large current. The volumes filled by oil are considered a "rock matrix" having mostly dielectric properties. The areas of contact of the individual grains are considered as narrow conductive passageways through the thin water films on the grain surfaces. These areas of contact form large sand clusters, covered by a layer of water, which are treated as large conductive passageways. The polarization of the saltwater-saturated clusters in this condition should be larger than that of the saturated oil, which occupies the rest of the porous space. In this model the induced polarization effect is caused mostly by the electrical double layers formed on the boundaries between the sand clusters and oil matrix. The conceptual model is capable of explaining the observed frequency dependence of the IP effect in structural terms. Our model suggests that at the critical water content, pore water becomes predominantly adsorbed on the solid surface. Therefore, a generic cation exchange capacity (CEC) effect and the electrical double layers on the surface of the sand clusters form a spatially distributed capacitor (see panel 2 in Fig. 3). The shape and composition of this spatially distributed capacitor define the nature of the IP effects in hydrocarbon-saturated sands. It is remarkable that the models of both the mineral rock with metal inclusions and of the reservoir-rock-like oiled sandstone could be described using formalism of GEMTIP.

### 2.4.1. Development of effective-medium model with random spherical inclusions for hydrocarbon-saturated media

Originally, a two-phase GEMTIP model [29,30] was used to determine mineralization or hydrocarbon saturation from the recorded electrical data:

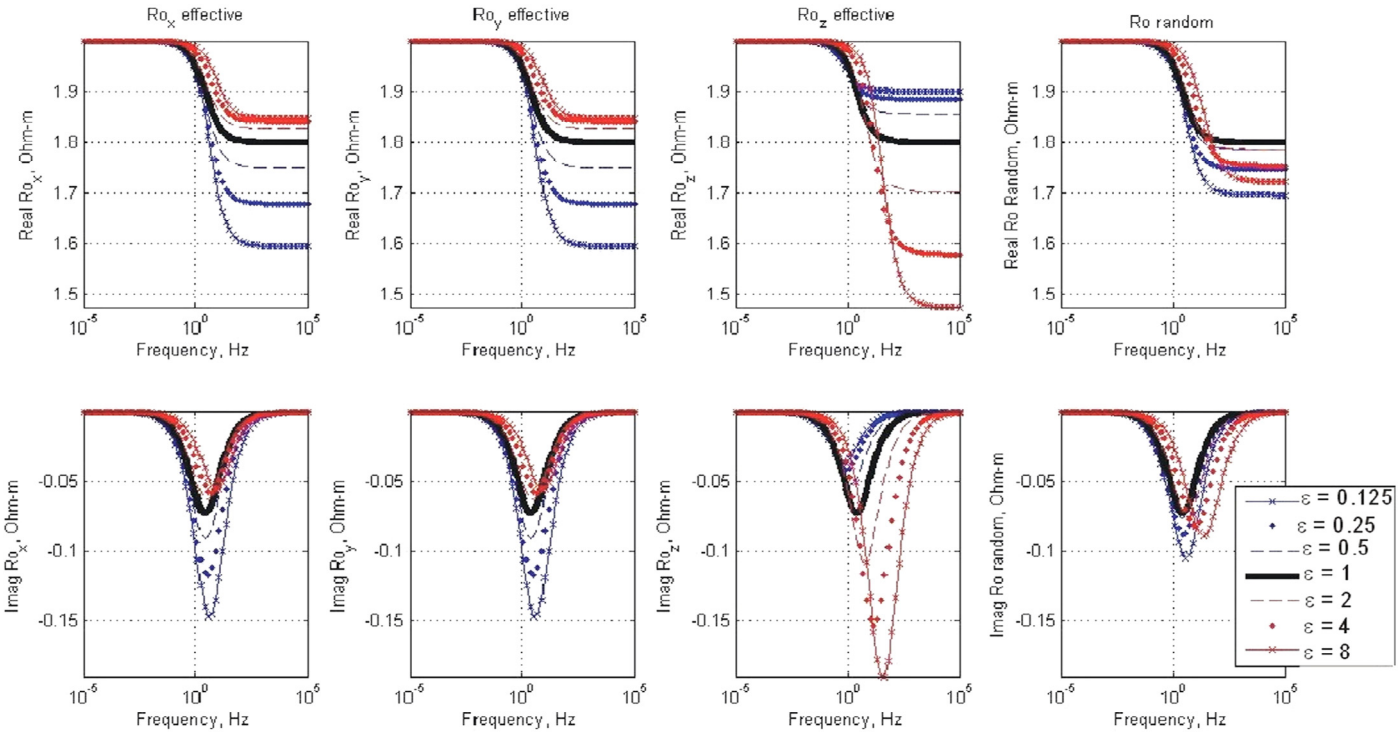


Fig. 2. Resistivity relaxation models of two-phase heterogeneous rock filled by ellipsoidal grains. Panels (a), (b), and (c) correspond to a model with the grains aligned along the Cartesian coordinates. Panel (d) presents the resistivity model for a case with random orientation of the grains. The upper panels show the real part of the complex effective resistivity, while the bottom panels present the imaginary part of the complex effective resistivity. The different curves in each panel correspond to the different ellipticities of the grains: ε = c/a = 5; 0.25; 0.5; 1; 2; 4; 8, respectively.

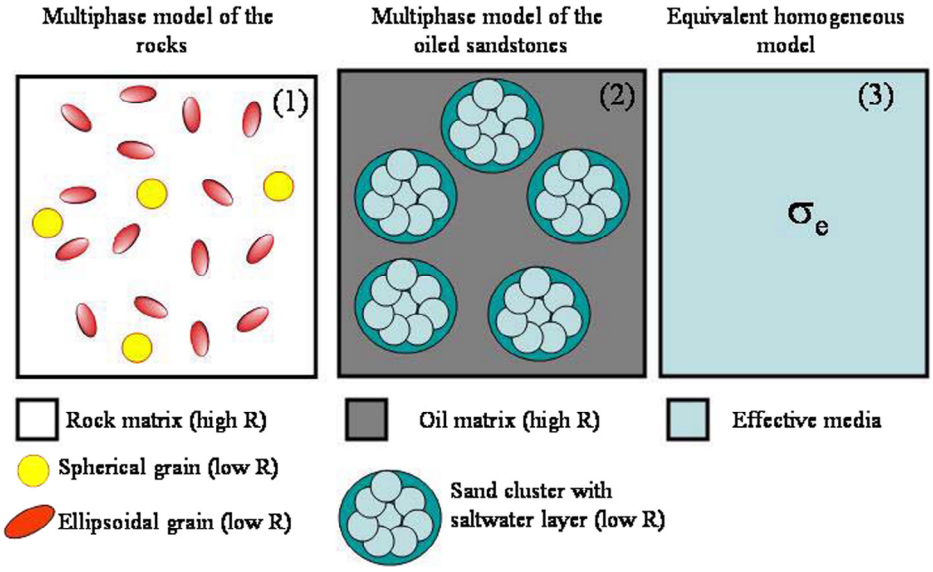


Fig. 3. Effective-medium model (3) of mineral rock (1) and oiled sandstone (2) samples.

$$\rho_{ef} = \rho_0 \left\{ 1 + f_l m_l \left[ 1 - \frac{1}{1 + (i\omega\tau_l)^{-C_l}} \right] \right\}^{-1}, \tag{23}$$

where:

$$m_l = 3\frac{\rho_0 - \rho_l}{2\rho_l + \rho_0} \text{ and } \tau_l = \left\{ \frac{a_l}{2\alpha_l}(2\rho_l + \rho_0) \right\}^{-C_l}, \tag{24}$$

where $\rho_{ef}$ [Ω-m] is the resulting effective resistivity, $\rho_0$ [Ω-m] is the matrix resistivity of the rock being modeled, $f_l$ is a volume fraction volume of a grain, $m_l$ is a grain chargeability, $\omega$ [Hz] is an angular frequency, $\tau_l$ [s] is a time constant, $C_l$ is a decay coefficient, $\rho_l$ [Ω-m] is a grain resistivity, $a_l$ [m] is a grain radius, and $\alpha_l$ is a surface polarizability coefficient.

This model was applied for GEMTIP fit of the experimental data at early stages of our research [32,33].

*2.4.2. Development of effective-medium model with random ellipsoidal inclusions for hydrocarbon-saturated media*

We consider now a medium with completely randomly oriented ellipsoids. The effective conductivity of this medium can be calculated by taking an average over the orientations. We obtain the following:

$$\rho_e = \rho_0 \left\{ \frac{1+\sum_{l=1}^{N} \frac{f_l m_l}{3}}{\sum_{a=x,y,z} \frac{2\rho_l+\rho_0}{3h_a}\left[1-\frac{1}{1+(-i\omega\tau_l)^{C_l}}\frac{2h_a}{\lambda_{la}\bar{a}_l(2\rho_l+\rho_0)}\right]} \right\}^{-1},$$

where

$$h_a = \rho_l + \gamma_{la}(\rho_0 - \rho_l).$$

The coefficients $\lambda_{la}$ and $\gamma_{la}$ are the structural parameters defined by geometrical characteristics of the ellipsoidal inclusions [30,31,33], and they are functions of ellipticity $e_l$. And $\bar{a}_l$ is an average value of the equatorial ( $a_{lx}$ and $a_{ly}$) and polar ( $a_{lz}$) radii of the ellipsoidal grains, $\bar{a}_l = (a_{lx}+a_{ly}+a_{lz})/3$. If all the grains are oriented in one specific direction, the effective conductivity of this medium will become anisotropic. Thus, the effective conductivity may be a tensor in spite of the fact that the background medium and all the grains are electrically isotropic.

We find that the following assumptions and notation are useful for practical modeling:

$$\frac{2h_a}{\lambda_{la}(2\rho_l+\rho_0)} = \frac{2[\rho_l+\gamma_{la}(\rho_0-\rho_l)]}{\lambda_{la}(2\rho_l+\rho_0)} \approx \frac{2\gamma_{la}}{\lambda_{la}} = r_a.$$

We can also consider that all inclusions in GEMTIP model are conductive, so:

$$\frac{2\rho_l+\rho_0}{3h_a} = \frac{2\rho_l+\rho_0}{3[\rho_l+\gamma_{la}(\rho_0-\rho_l)]} \approx \frac{1}{3\gamma_{la}}, \text{ and}$$

$$m_l = 3\frac{\rho_0-\rho_l}{\rho_0+2\rho_l} \approx 3.$$

Finally we have:

$$\rho_e = \rho_0 \left\{ 1 + f_l \sum_{\alpha=x,y,z} \frac{1}{3\gamma_{l\alpha}} \left[ 1 - \frac{1}{1+(-i\omega\tau_l)^{C_l}} \frac{r_\alpha}{\bar{a}_l} \right] \right\}^{-1} \quad (25)$$

We use the expression (25) for latest inversion studies of IP effect in HC saturated media.

## 3. Experimental study of the IP effect in HC-saturated sands and sandstones

For initial studies we prepared two types of samples for a measurement. The first type is represented by the sandstone samples. The second type of samples was formed by artificially prepared water and oil-saturated sands and oiled sands. We designated the second type of samples as cartridges or artificial rocks in later research. The sample preparation is described in details in Burtman [32]. We used a Zonge GDP16 CR measurement setup to test the complex resistivity (CR) of HC-saturated rock samples at a frequency range of 0.0156–9216 Hz.

Fig. 4 presents the recorded imaginary resistivity vs. frequency curves for samples SCO (sand–cartridge–oil) and SCW (sand–cartridge–water) respectively. It is evident that the resistivity relaxation curves for both the SSO and SCO samples are characterized by a pronounced IP effect.

In the period of initial studies we explored the possibility of fabricating HC saturated samples and detecting the IP effect in these samples using standard geophysical EM equipment. We developed the experimental route for preparing reservoir and artificial rocks. Artificial rocks were prepared from chemically pure substances without metal inclusions and observed large IP responses in HC-saturated rocks. We attributed an observed IP effect to membrane polarization phenomena. At this stage we began to develop the Effective Medium Induced polarization (GEMTIP) model to analyze IP effect in HC-saturated sands and sandstones.

The initial experiments were followed up by advanced studies which included two parts. In the first part, the low frequency study, we conducted a detailed experimental study of the IP effect in oil-saturated rock samples at frequencies below 100 Hz. In particular, we obtained experimental data on (i) evaluating the errors in the CR measurements, (ii) dependence of the CR measurements on pH, and (iii) the shift of the IP signal at a low frequency range, while decreasing pH. The measurements were conducted in the facilities of the Zonge Engineering and Research Organization.

In the second part, the high-frequency study, we investigated induced polarization (IP) effects in hydrocarbon-bearing artificial rocks at frequencies greater than 100 Hz. We examined the instrumental and electrode phase responses of Zonge International's complex resistivity (CR) system, and optimized the

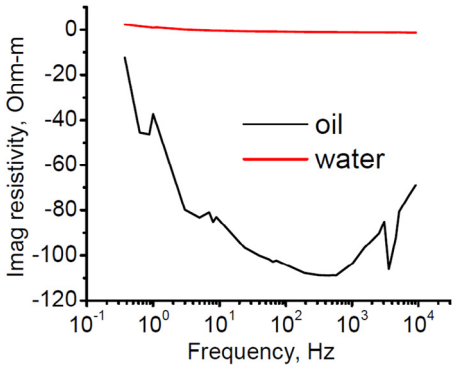


Fig. 4. The imaginary parts of the resistivity vs. frequency curves for the water (SCW) and oil–saturated sand (SCO) cartridges.

performance of the Zonge system for IP measurements above the 1 mHz–10 kHz frequency range. The reliability of the high-frequency IP measurements were confirmed by independent measurement of the same samples using the Novocontrol BDS 80 system. These results confirm the presence of IP effects in hydrocarbon-bearing rocks, and suggest the necessity to account for IP effects in the interpretations of electromagnetic data.

### 3.1. Low-frequency studies: complex resistivity (CR) data statistics

The testing protocol involved testing the SCO and SSO samples five times in sequence. Each frequency was taken once, but the CR at the whole frequency range was repeated five times to obtain the representative statistics. The shunt resistance (resistance equal to the resistance of a sample) was manually set every time the resistance of the sample was changed with the frequency. The measurement time for the entire frequency range measurement was about 25–35 minutes. The current during CR measurements did not exceed 0.2 mA. The time interval between adjacent measurements was more than 10 s, which should have allowed us to consider every measurement event to be independent and not correlated with the previous measurement. Indeed, the typical relaxation time in mineral rock samples is 1 s. We have analyzed some statistical information about the observed data using the following conventional statistical parameters. The standard deviation (SD) is calculated as follows:

$SD = \sqrt{Var}$, where

$$Var = \frac{1}{n-1}\sum_{i=1}^{n}(X_i - \bar{X})^2.$$

In this formula n is the sample size, and $\bar{X}$ is the mean. The standard error of the mean (SE) is calculated as follows:

$$SE = \frac{SD}{\sqrt{n}}.$$

The averaged data points were plotted with SD and SE error bars for each data set.

We examined the sand–cartridge–oil (SCO) samples. The CR data were used for statistical analysis and plotted in Fig. 5(A) and 5(B).

The fact that $\rho_0$ does not change essentially with time means that the sample is stable with respect to the diffusion of electrolytes, which is due to the fact that the KCl solution (used to establish a contact in the measurement setup) does not wet the sample. It is due to oil, which saturates the sample and forms a "protection" film on the sample surface. Also, the SCO sample plugs provide an additional protection against electrolyte diffusion. Therefore, the HC-saturated samples, both SSO and SCO, are electrochemically stable for long-time measurement.

Fig. 5(C) and 5(D) summarizes the observed data and correspondent statistics. A comparison of SE to an average value shows that the error bars for amplitude of the apparent resistivity (0.9–1.27%) and for real resistivity (0.22–1.31%) are very similar. The same relationship between the average values and SE was observed for error bars calculated for phase

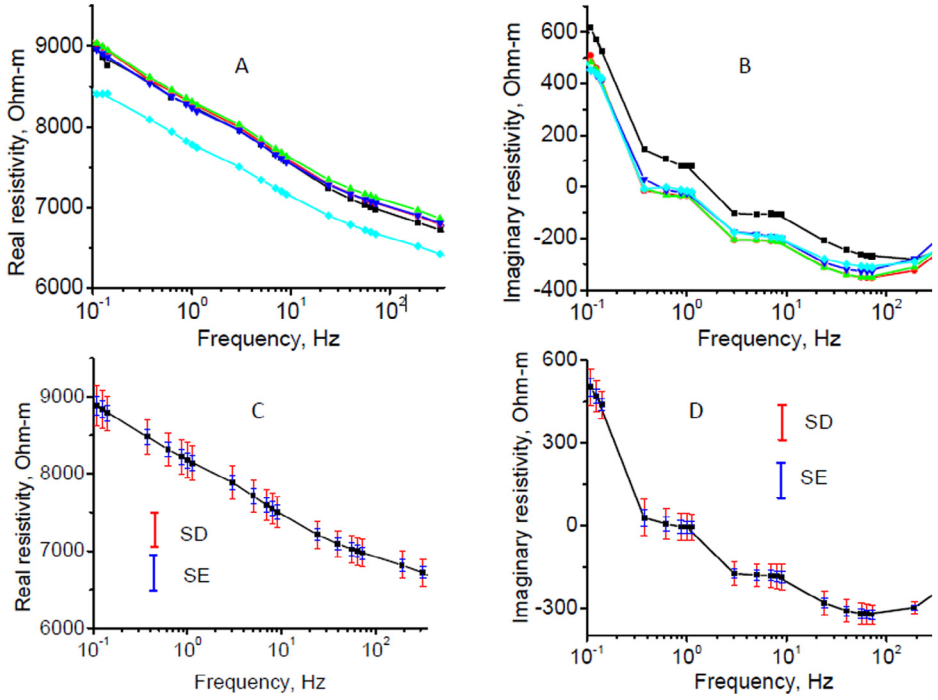


Fig. 5. Spectral real and imaginary apparent resistivity plots for sand–cartridge–oil (SCO) samples. (A) Real resistivity spectra measured 5 times in sequence. (B) Imaginary resistivity spectra measured 5 times in sequence. (C) Standard deviation (SD) and standard error (SE) for the mean values of real resistivity spectra measured 5 times in sequence. (D) Standard deviation (SD) and standard error (SE) for mean values of imaginary resistivity spectra measured 5 times in sequence.

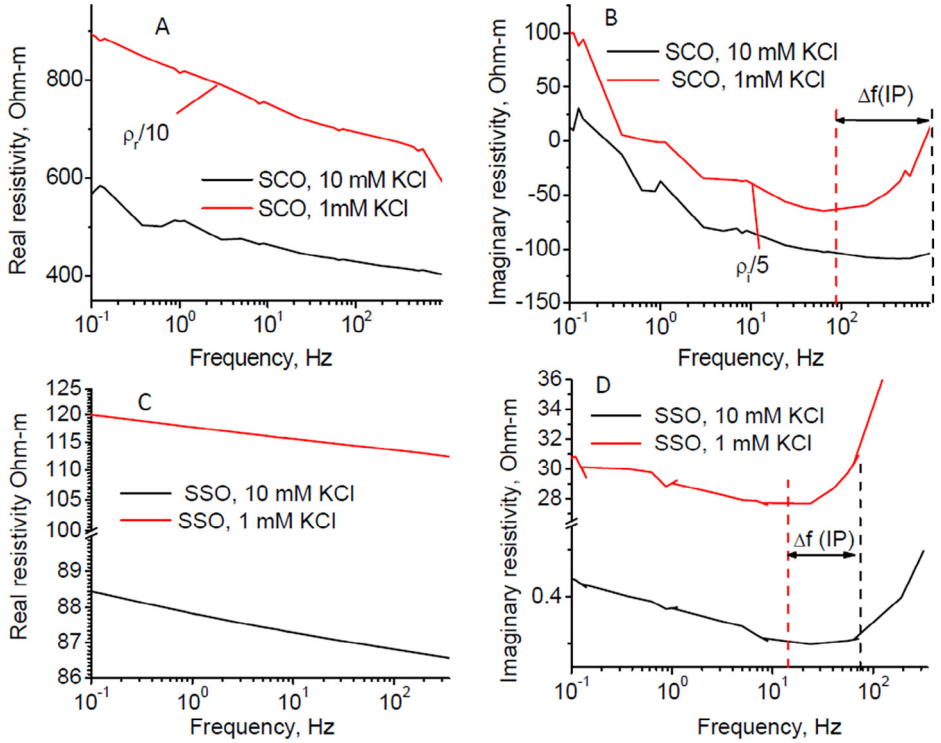


Fig. 6. (A) The real parts of the resistivity vs. frequency curves for the sand–cartridge–oil (SCO) samples, which were prepared using different saltwater pH (1 and 10 mM). (B) The imaginary parts of the resistivity vs. frequency curves for the sand–cartridge–oil (SCO) samples, which were prepared using different saltwater pH (1 and 10 mM). (C) The real parts of the resistivity vs. frequency curves for the sandstone–oil (SSO) samples, which were prepared using different saltwater pH (1 and 10 mM). (D) The imaginary parts of the resistivity vs. frequency curves for the sandstone–oil (SSO) samples, which were prepared using different saltwater pH (1 and 10 mM).

(1.08–10%) and imaginary resistivity (1.01–11%). A small deviation in error bars could be explained by small changes in $\rho_0$, which was decreasing with time due to a negligibly small charge trapped in the sample. It is worth noting that some types of mineral rock samples, which were tested as a part of the control experiments, do not show such stability toward KCl electro-diffusion damage.

### *3.2. Low-frequency studies: changes in complex resistivity (CR) upon pH variation*

We conducted a study of SCO samples with variable saltwater pH. This study was critical in order to verify the feasibility of IP method in HC exploration. To reproduce this observation in our experimental measurements of the reservoir rock samples, we tested two SCO samples and two SSO samples. In each case we changed the pH of the saltwater used for the sample preparation only. Fig. 6(A) and 6(B) presents the real and imaginary spectra of SCO samples with different saltwater pH absorbed on the sand cluster.

Similar behavior was observed in the SSO samples. Fig. 6(C) and 6(D) compares the real and imaginary spectra of the SSO samples with different saltwater pH, which was the same as for the SCO samples. The observed experimental results correspond well to those reported in the literature (e.g., Slater, 2005): the frequency of the IP peak decreases with the decrease in the pH of the electrolyte.

## 4. Complex resistivity measurements of internal induced polarization of oil-based mud

### *4.1. Low-frequency studies: complex resistivity (CR) studies*

For this study, Baker Hughes provided an oil-based mud, which we then used in our high-frequency IP experiments. Oil-based mud is a drilling fluid, whose base is a petroleum product similar to diesel fuel. The exact composition of the oil-based mud was not disclosed. The sample holder was assembled as an empty PVC cartridge with ribbon O-rings on the side attached to the OYO electrodes using mounting ribbons. Different liquids could be placed in the sample holder through a hole drilled in the PVC wall. The PVC tube was first mounted between the OYO electrodes, and then filled with liquid using a syringe. The cotton pads were not used for contacts. The same syringe was also used to evacuate the liquids from the PVC tube. First, tap water (TW) and distilled water (DW) were tested as control experiments. Following these tests, the oil-based mud sample was measured. Results are shown in Fig. 7.

The following DC resistivities were used for calculating the complex resistivity: $R_{DC}^{\text{oil-mud}} = 106.8$ kΩ/m, $R_{DC}^{DW} = 91.4$ kΩ/m, $R_{DC}^{TW} = 15.6$ kΩ/m, and $R_{DC}^{\text{OYO-OYO}} = 51.$ kΩ/m. We observed the internal IP of the sample to be much larger than the external IP, implying that polarization due to the optimized CR system and OYO electrodes was negligible. We also noted that the tap and

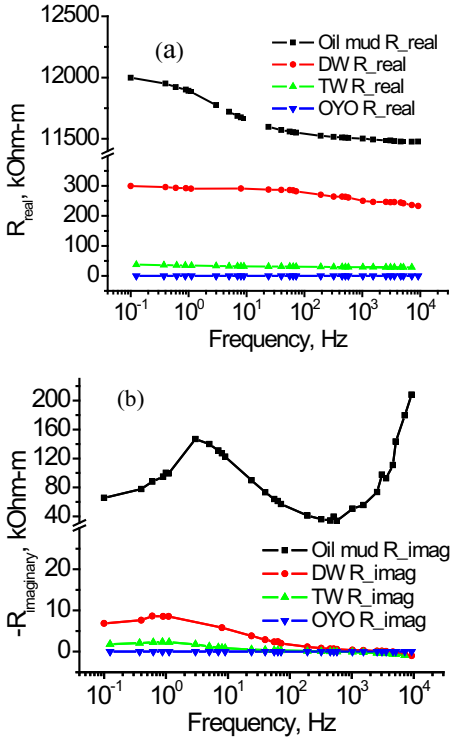


Fig. 7. CR(ω) measurments of mud oil based mud (oil mud) vs. tap water (TW) and distilled water (DW), and OYO electrodes in face-to-face configuration. Upper panel (a) shows the real resistivity, and the bottom panel (b) shows the imaginary resistivity.

distilled water polarization from 1 kHz was also negligibly small. The oil-based mud showed a well pronounced peak rising from 1 kHz and extending to higher frequencies. It is obvious from Fig. 7 that the electrode-related artifacts are practically negligible compared to the oil-based mud sample's complex resistivity response. This is similar to a conclusion that we previously reached for hydrocarbon-saturated rocks [32].

### *4.2. High-frequency studies: dielectric spectroscopy of oil-based mud*

The dielectric spectrum exhibits relaxation for most of organic solvents and suspensions. It is well known that the real part of the complex resistivity is related to the resistivity and loss terms, and the imaginary part is related to the polarization. In the case of the complex dielectric constant, the real part is related to the polarization and the imaginary part is related to the resistivity and loss terms. The dielectric spectrum of the oil-based mud sample was measured using a Novocontrol BDS 80 system. The frequency dependence of ε′, as shown in Fig. 8a, supports our initial interpretation that IP responses should be expected in oil-based mud samples at high frequencies. The dielectric constant ε′ is related to the polarization strength and can be converted to imaginary resistivity. These results can then be compared to our complex resistivity results from the Zonge CR system in Fig. 8b.

Despite instrumental and methodological differences between these two measurements, it is apparent that the imaginary resistivity calculated from the ε′ measurements follows the trend

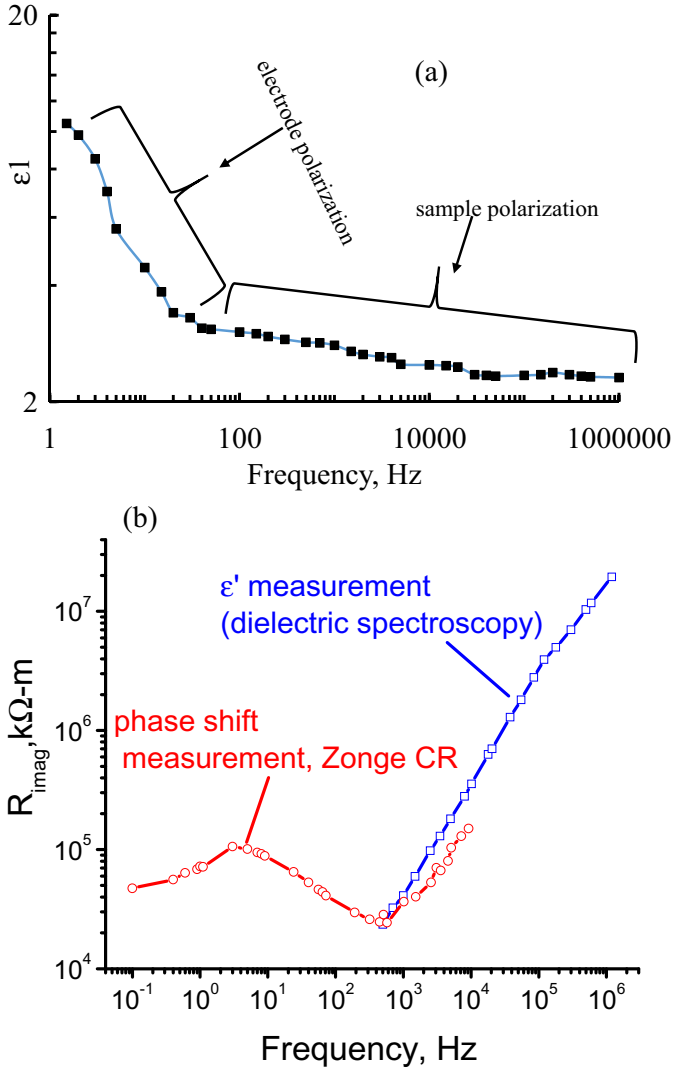


Fig. 8. Upper panel (a): Dielectric function (ε′) of the oil-based mud (OBM) sample measured using dielectric spectroscopy. Bottom panel (b): Comparison of the imaginary resistivity obtained by the CR(ω) and dielectric spectroscopy measurements.

observed in CR measurements, i.e., the nonlinearity of the imaginary resistivity spectrum observed in the 100 Hz–10 kHz range is reproduced in independent measurement. This nonlinearity continues to grow at elevated frequencies for the dielectric measurements.

To summarize study of oil-based muds, we measured the IP responses for oil-based mud, which showed an IP response from 100 Hz to MHz frequencies. As such, we have experimentally shown the need to account for IP effects in reservoir rocks. This will be particularly important for interpretation of induction well logs. That said, further research is required to fully understand the frequency-dependence of different polarization mechanisms that occur in reservoir rocks. Results shown in this section have validated the reliability of the high-frequency IP measurements that were independently confirmed by measuring the CR spectrum of the same samples using the Novocontrol BDS 80 system.

## 5. Experimental study of the IP effect in the HC-saturated carbonate rocks

In the paper presented at the EAGE 2013 meeting in London [41], we demonstrated that carbonate rock samples, typical of a HC reservoir, showed in the laboratory distinct IP responses that were statistically repeatable. The reservoir rocks saturated with crude oil were observed to have complex resistivity (CR) spectra different and distinct from the same reservoir rocks saturated with brine. Therefore, it was shown that IP methods had the potential to provide a basis for in situ fluid discrimination. We demonstrated also that, using the analysis based on Generalized Effective Medium Theory of Induced Polarization (GEMTIP) one can invert the observed CR spectra for meaningful rock and fluid properties, such as fluid saturations and porosity. It was shown that the GEMTIP-derived chargeability can be directly correlated with porosity for the selected carbonate reservoir rock formations. GEMTIP based inversion also recovers the resistivities of the fluids in the rock samples, thereby making it feasible to produce 3D models of porosity and fluid (oil and water) saturations from the 3D models of resistivity and chargeability, as recovered from the GEMTIP-based 3D inversion of large-scale field IP data.

### *5.1. Experimental setup, sample preparation, and measurements*

We have developed a complex resistivity (CR) measurement system consisting of a waveform generator, spectrum analyzer, PC control, and rock sample holder [41]. The methodology of CR measurements with TechnoImaging's CR system can be described as follows: (a) the rock sample is mounted between two electrodes in a sample holder; (b) the frequency range is preselected from 0.01 Hz to 1 kHz.; (c) a sinusoidal waveform of a preset frequency is transmitted to the sample and to the reference resistor (designated here as Rref); (d) the value of Rref is chosen to be close to the sample's resistance; (e) the amplitude of the sinusoidal waveform is the sample's resistance; (e) the amplitude of the sinusoidal waveform is chosen to provide the maximum signal-to-noise ratio from 200 mV to 10 V; (f) the response from the sample and Rref is analyzed on the oscilloscope; (g) the difference in phase and amplitude between the two sinusoidal waveforms is recorded and stored for each current frequency; (h) these differences are converted into the pairs of real and imaginary parts of complex resistivity for each frequency. When collated, these individual CR measurements form the CR spectra.

We have conducted laboratory-based analyses of reservoir rock and fluid samples from the selected carbonate reservoirs [41]. All samples were saturated with brine from the respective origin wells, and then by their respective crude oil in a vacuum system. In addition, we have fabricated and measured the CR responses for artificial rocks composed of pure sand and saturated with brine, and for crude oil from the selected reservoirs, respectively.

As an example, Fig. 9 presents a comparison of the complex resistivity spectra for a rock sample of the first reservoir saturated in brine (blue line) and crude oil (red line). The upper panel shows the real resistivity and the bottom panel shows the imaginary resistivity as the functions of frequency. We have analyzed some statistical information about the observed data using the following conventional statistical parameters. The averaged data points were plotted with standard deviation (SD) and standard error of the mean (SE) error bars for each data set. The results of CR measurements of the rock samples saturated in brine and crude oil demonstrated increasing of resistivity and a high-frequency shift in the IP peak with oil saturation.

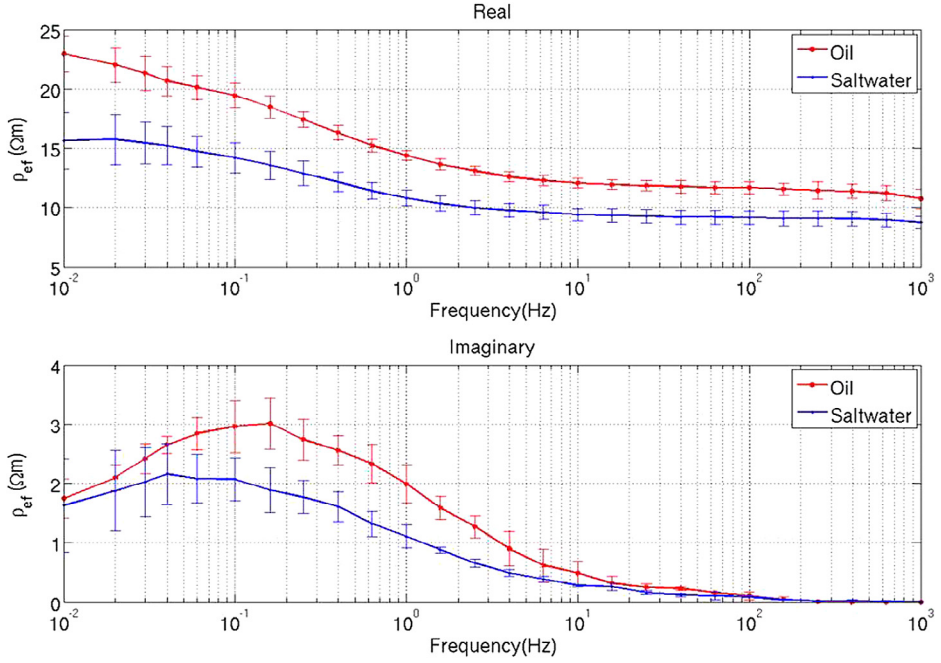


Fig. 9. Comparison of the complex resistivity spectra for a reservoir rock sample saturated in brine (blue line) and crude oil (red line). The error bars show the standard error of the mean values.

It was demonstrated in Zhdanov (2008, 2009) [28,30] that the IP phenomenon can be mathematically explained by a composite geoelectrical model of reservoir formations. This model is based on the effective-medium approach, which takes into account both the volume polarization and the surface polarization of the porous space. The new composite geoelectrical model allows us to model the relationships between the physical characteristics of different types of rocks and minerals (e.g., conductivities, porosity, and polarizability) and the parameters of the relaxation model. A new generalized effective-medium theory of the induced polarization effect (GEMTIP), introduced in the cited papers, treats in a unified way different complex multiphase composite models of the rocks. In our analyses, we have used the GEMTIP model consisting of a medium filled with randomly oriented ellipsoidal inclusions. Note that the ellipsoidal inclusions can be used to describe a great variety of different shapes ranging from the prolate ellipsoids, approximating thin laminating layers, to the oblate relatively thin ellipsoids approximating thin capillaries in the porous space.

The GEMTIP model parameters include the DC resistivity, $\rho_0$, the chargeability parameter, the time constant, and the decay constant of the CR curves. As discussed in Zhdanov (2008) [30], the chargeability term is a linear function of the fraction volume of the inclusions, and therefore can be expressed as a linear function of the porosity. Thus, we have demonstrated that it is possible to recover a 3D porosity model from a transform of the 3D chargeability model. When this is interpreted with the 3D resistivity model simultaneously recovered from the 3D inversion of IP data, this suggests that it is possible to recover 3D fluid saturation models. According to the GEMTIP approach, the effective resistivity model for a medium with randomly oriented ellipsoidal inclusions is given by the following equation:

$$\rho_{ef} = \rho_0\left(1+\frac{p}{9}\sum_{\alpha=x,y,z}\frac{1}{\gamma_\alpha}\left[1-\frac{1}{1+s_\alpha(i\omega\tau_l)^{C_l}}\right]\right)^{-1}, \tag{26}$$

where $\rho_{ef}$ [Ω-m] is the resulting effective resistivity, $\rho_0$ [Ω-m] is the matrix resistivity of the rock being modeled, $p$ is a chargeability parameter, $\omega$ [Hz] is an angular frequency, $\tau_l$ [s] is a time constant, $C_l$ is a decay coefficient. The coefficients $\gamma_\alpha$ and $s_\alpha$ are the structural parameters defined by geometrical characteristics of the ellipsoidal inclusions used to approximate the porous space [30].

We introduce a vector, $m$, of the unknown model parameters:

$$\mathrm{m} = [\mathrm{p}, \tau, \mathrm{C}, \gamma, \mathrm{s}],$$

and a vector, $d$, of the observed data (i.e., the values of CR as a function of frequency):

$$\mathrm{d} = [\rho_{ef}(\omega_1), \rho_{ef}(\omega_2), \ldots \rho_{ef}(\omega_n),]$$

Using these notations, we can write equation (1) in the following form:

$$\mathrm{d} = \mathrm{A}(\mathrm{m}) \tag{27}$$

To find the parameters of the GEMTIP model, we should solve equation (25) with respect to m. We use the inversion algorithm based on the regularized conjugate gradient (RCG) method [42]. The RCG method is an iterative solver, which updates the model parameters on each iteration using conjugate gradient method.

As an example, Fig. 10 presents the observed and GEMTIP-predicted data for a rock sample saturated in crude oil from the first carbonate reservoir. We can see a very good fit of the

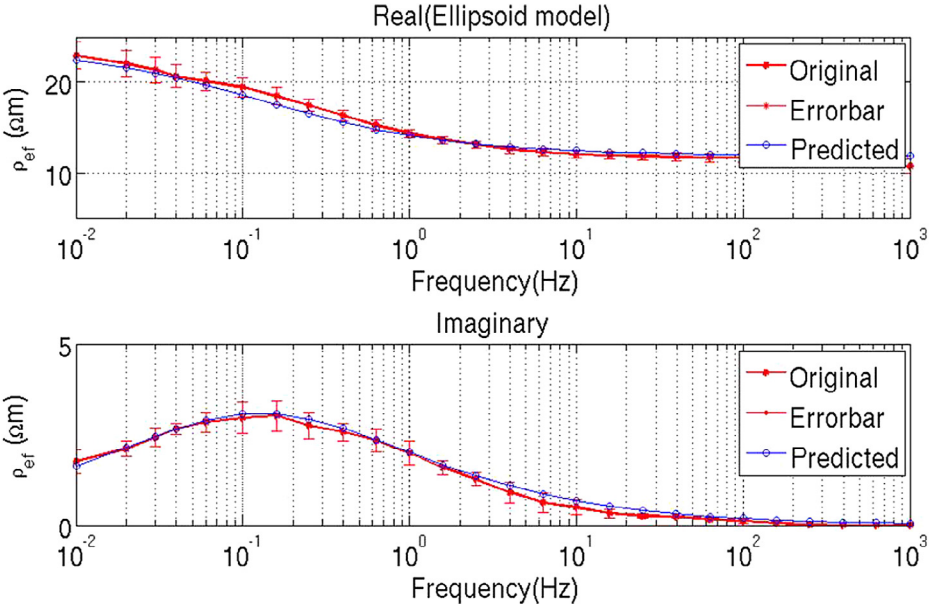


Fig. 10. Observed (red) and GEMTIP-predicted (blue) real and imaginary spectra for a reservoir rock sample saturated in crude oil.

observed CR data by the GEMTIP model in this case. Similar results were obtained for rock samples originated from the second carbonate reservoir studied in this research.

Thus, we have demonstrated that the carbonate rocks saturated with crude oil are observed to have different and distinct CR spectra than the same reservoir rocks saturated with brine. Therefore, the IP method can provide a basis for in situ fluid discrimination; however, the challenge then remains to invert the observed CR spectra for meaningful rock and fluid properties such as fluid saturations and porosity. The GEMTIP analysis demonstrates that the GEMTIP-derived chargeability can be directly correlated with porosity for the selected carbonate reservoir formations. GEMTIP-based inversion also recovers the resistivities of the fluids in each sample. Finally, we suggest that it is feasible to produce 3D models of the porosity and fluid (oil and water) saturations from the 3D models of resistivity and chargeability as recovered from the GEMTIP-based 3D inversion of the field IP data.

## 6. Discussion and conclusions

The IP effect has been studied and practically used for hydrocarbon exploration for many years (e.g., Zonge, 1983 [3]; Seigel et al., 2007 [43]; Davydycheva et al., 2006 [27]). However, the theoretical and experimental study of the IP effect in reservoir rocks remains in the very initial stage, partly due to the lack of systematic research of this phenomenon. The results presented in this paper contribute to a better understanding of the nature of the IP effect in HC reservoirs. We have developed a model in the context of the effective media approach to describe a mechanism of membrane polarization in oil-saturated sands and a methodology for experimental study of this effect.

First, we observed a pronounced IP effect in sandstone samples which were artificially saturated with synthetic oil. A careful comparison of the EM response from the oil-saturated sandstones with control samples (sand cartridges) demonstrates that the observed IP effect could be attributed to membrane polarization phenomena, and not to the response from metal inclusions, electrodes, or geometric factors. The difference in shape and amplitude of the peak of the IP response is attributed to the difference in structural features between the controlled sample and in oil-saturated sandstones.

Second, our study showed that the membrane polarization phenomenon is closely related to a spatial configuration of the charged membrane associated with the double electrical layers formed at the surface of the solid phase and on the large sand grain clusters.

Third, we applied the effective-medium approach, GEMTIP, to analyze the complex resistivity of the oiled sandstone. The numerical comparison of the experimental data with the data predicted by the GEMTIP model, based on the rigorous solution of Maxwell's equations for a heterogeneous medium, has proved the validity of the GEMTIP model for analysis of the membrane polarization phenomenon.

Fourth, we demonstrated that the carbonate rocks saturated with crude oil were characterized by CR spectra different and distinct from the same reservoir rocks saturated with brine.

These experimental observations and modeling study confirm earlier geophysical experiments with the application of the IP method for HC exploration. As laboratory studies have shown, a description of IP in terms of complex electrical conductivity enables access to various structural characteristics pertinent to practical issues such as hydrocarbon mapping. In particular, analysis in terms of real and imaginary conductivity components offers improved lithologic characterization, since the IP effect could be separated from electrolytic and surface conduction effects [44]. Note that it was demonstrated in the paper by Burtman et al. (2014) [45] that one can observe significant induced polarization effects in shale reservoir rocks, which can be used in exploration for unconventional reserves as well.

Thus, this paper overviews the studies of the IP effect in HC bearing reservoir rocks conducted by the University of Utah Consortium for Electromagnetic Modeling and Inversion (CEMI) and TechnoImaging over the last decade. The results of these studies provide an experimental and theoretical basis for the use of the IP method for HC exploration and production monitoring. The results of these research demonstrate also that the GEMTIP model plays a critical role in the solution of this problem.

## Acknowledgments

The authors acknowledge the support of the University of Utah Consortium for Electromagnetic Modeling and Inversion (CEMI). The authors acknowledge Saudi Aramco and Baker Hughes for providing the samples of carbonate rocks and oil based mud samples, and TechnoImaging for support of this research and permission to publish. Special thanks to Dr. Alberta Marsala for fruitful discussions.

## References

[1] V. Vacquier, C.R. Holmes, P.R. Kintzinger, M. Lavergne, Prospecting for groundwater by induced electrical polarization, Geophysics 23 (1957) 660–687.
[2] D.J. Marshall, T.R. Madden, Induced polarization, a study of its causes, Geophysics 24 (1959) 790–816.
[3] K.L. Zonge, Case histories of an electromagnetic method for petroleum exploration. Proprietary Data Sale, Zonge Engineering and Research Organization, Inc., 1983.
[4] B.K. Sternberg, D.Z. Oehler, Induced polarization in hydrocarbon surveys: Arkoma Basin case histories, in: S.H. Ward (Ed.), Induced Polarization: Applications and Case Histories, vol. 4, Society of Exploration Geophysicists, 1990.
[5] J.N. Towel, R.G. Anderson, W.H. Pelton, G.R. Olhoeft, D. LaBrecque, Direct detection of hydrocarbon contaminants using induced polarization method. 55th Annual International Meeting, SEG, Expanded Abstracts, 145–147, 1985.
[6] J.D. Klein, W.R. Sill, Electrical properties of artificial clay-bearing sandstone, Geophysics 47 (1982) 1593–1605.
[7] J.S. Sumner, Principles of Induced Polarization for Geophysical Exploration, Elsevier Scientific Publishing, Amsterdam, 1976.
[8] C. Schlumberger, Etude Sur la Prospection Electrique du Soussol, Gauthier Villars, Paris, 1920.
[9] J.R. Wait, The variable-frequency method, in: J.R. Wait (Ed.), Overvoltage Research and Geophysical Applications, Pergamon, 1959.
[10] D.F. Bleil, Induced polarization, a method of geophysical prospecting, Geophysics 18 (1953) 636–661.

[11] A.A. Ogilvy, E. Kuzmina, Hydrogeological and engineering-geologic possibilities for employing the method of induced potentials, Geophysics 37 (1972) 839–861.
[12] K.K. Roy, H. Elliot, Model studies on some aspects of resistivity and membrane polarization behavior over a layer Earth, Geophys. Prospect. 28 (1980) 759–775.
[13] H. Vanhala, H. Soininen, Laboratory technique for measurement of spectral induced polarization response of soil samples, Geophys. Prospect. 43 (1995) 655–1376.
[14] M.H. Cohen, Scale invariance of the low frequency electrical properties of inhomogeneous materials, Geophysics 46 (1981) 1057–1059.
[15] G.V. Keller, F.C. Frischknecht, Electrical Methods in Geophysical Prospecting, vol. 10, Pergamon, 1966.
[16] M. Waxman, L.J.M. Smits, Electrical conductivities in oil-bearing shaly sands, Soc. Pet. Eng. J. 243 (1968) 107–122.
[17] M.H. Waxman, E.C. Thomas, Electrical conductivities in shaly sands, J. Petrol. Technol. 257 (1974) 213–225.
[18] E.I. Parkhomenko, Electrification Phenomena in Rocks, Plenum Press, New York, 1971.
[19] V.N. Dakhnov, Geophysical Well Logging, Colorado School of Mines, 1962.
[20] O.A. de Lima, M.M. Sharma, A generalized Maxwell-Wagner theory for membrane polarization in shaly sands, Geophysics 58 (1992) 431–440.
[21] F.K. Boadu, B. Seabrook, Estimating hydraulic conductivity and porosity of soils from spectral electrical response measurements, J. Environ. Eng. Geophys. 5 (2000) 1–9.
[22] G.R. Olhoeft, Low frequency electrical properties, Geophysics 50 (1985) 2492–2503.
[23] O. Mazac, W.E. Kelly, I. Landa, A hydrogeophysical model for relations between electrical and hydraulic properties of aquifers, J. Hydrol. 79 (1985) 1–9.
[24] F.D. Borner, J.R. Schopper, A. Weller, Evaluation of transport and storage properties in the soil and groundwater zone from the induced polarization measurements, Geophys. Prospect. 44 (1996) 583–601.
[25] T.L. Dobecki, P.R. Roming, Geotechnical and groundwater geophysics, Geophysics 50 (1985) 2621–2663.
[26] E.D. Tune, D.H. Daggar, Analysis of induced polarization and radiometric logs from a test borehole in Hawkesbury sandstone, Explor. Geophys. 21 (1990) 53–63.
[27] S. Davydycheva, N. Rykhlinski, P. Legeido, Electrical-prospecting method for hydrocarbon search using the induced-polarization effect, Geophysics 71 (2006) G179–G189.
[28] M.S. Zhdanov, Geophysical Electromagnetic Theory and Methods, Elsevier, 2009. 849 pp.
[29] M.S. Zhdanov, Generalized effective-medium theory of induced polarization. 76th Annual International Meeting, SEG, Expanded Abstracts, 805–809, 2006.
[30] M.S. Zhdanov, Generalized effective-medium theory of induced polarization, Geophysics 73 (2008) F197–F211.
[31] M.S. Zhdanov, Geophysical technique for mineral exploration and discrimination based on electromagnetic methods and associated systems (2008). US Patent 7,324,899 B2.
[32] V. Burtman, A. Gribenko, M.S. Zhdanov, Induced polarization in hydrocarbon-saturated sands and sandstones: experimental study and general effective medium modeling. SEG International Exposition and Annual Meeting, Houston, 774–777, 2009.
[33] V. Burtman, A. Gribenko, M.S. Zhdanov, Advances in experimental research of induced polarization effect in reservoir rocks. 80th Annual International Meeting, SEG, Denver, Colorado, 2010.
[34] V. Burtman, M. Endo, M.S. Zhdanov, T. Ingeman-Nielsen, High frequency induced polarization measurements of hydrocarbon-bearing rocks. 81st Annual International Meeting, SEG, San Antonio, Texas, 2011.
[35] A. Revil, W. Woodruff, C. Torres-Verdín, M. Prasad, Complex conductivity tensor of anisotropic hydrocarbon-bearing shales and mudrocks, Geophysics 78 (2013) D403–D418, doi:10.1190/geo2013-0100.1.
[36] A. Revil, K. Koch, K. Holliger, Is it the grain size or the characteristic pore size that controls the induced polarization relaxation time of clean sands and sandstones?, Water Resour. Res. 48 (2012) W05602, doi:10.1029/2011WR011561.
[37] A. Sihvola, P.J.B. Clarricoats, E.V. Jull (Eds.), Electromagnetic Mixing Formulae and Applications, IEEE Electromagnetic Waves Series No. 47, 2000.
[38] Y. Luo, G. Zhang, Theory and application of spectral induced polarization: SEG, 1998.
[39] J.R. Wait, Geo-Electromagnetism, Academic Press, 1982.
[40] C.M. Prince, R. Ehrlich, Y. Anguy, Analysis of spatial order in sandstones II: grain clusters, packing flaws, and the small-scale structure of sandstones, J. Sediment. Res. A65 (1995) 13–28.
[41] M.S. Zhdanov, V. Burtman, A. Marsala, Carbonate reservoir rocks show induced polarization effects, based on generalized effective medium theory. EAGE International Exposition and Annual Meeting, London, 2013.
[42] M.S. Zhdanov, Geophysical Inverse Theory and Regularization Problems, Elsevier, Amsterdam, 2002.
[43] H.O. Seigel, M. Nabighian, D. Parasnis, K. Vozoff, The early history of the induced polarization method, TLE 26 (2007) 312–321.
[44] A. Kemna, A. Binleyz, L. Slater, Crosshole IP imaging for engineering and environmental applications, Geophysics 69 (2004) 97–107.
[45] V. Burtman, H. Fu, M.S. Zhdanov, Experimental study of induced polarization effect in unconventional reservoir rocks, Geomaterials 4 (4) (2014) 117.